Chemical Conversion Reaction between CdS Nanobelts and ZnS Nanobelts by Vapor Transport

Jin Young Lee, Dae Sung Kim, and Jeunghee Park*

Department of Chemistry, Korea University, Jochiwon 339-700, Korea

Received March 25, 2007. Revised Manuscript Received May 17, 2007

Single-crystalline wurtzite CdS nanobelts are completely converted into single-crystalline wurtzite ZnS nanobelts by Zn vapor transport (at 800 °C). In contrast, the ZnS nanobelts are not completely transformed into CdS nanobelts by Cd vapor transport but yield Cd-doped (up to 60%) ZnS nanobelts (at 1000 °C). This result indicates that the conversion reaction of the CdS nanobelts into the ZnS nanobelts takes place more efficiently, as compared to the opposite reaction. At temperatures lower than the conversion temperature, a CdS−ZnO nanobelt−nanowire hybrid structure grew, in which the ZnO nanowires were aligned in the [0001] direction of the CdS nanobelts. We suggest that the conversion reaction of the wurtzite CdS structure proceeds preferentially through their polar (001) planes.

Introduction

Since the discovery of carbon nanotubes (CNTs), a tremendous amount of research has been conducted on the synthesis and utilization of 1-D nanostructures (e.g., nanowires and nanobelts) as well-defined building blocks for assembling active and integrated nanodevice systems.[1] Nanowires/nanobelts made of CdS (E_g = 2.42 eV at room temperature) and ZnS (E_g = 3.6 eV at room temperature), which are important wide band gap II−VI semiconductor materials, have been the object of particular attention because of their unique properties and wide range of applications in sensors, lasers, waveguides, and optoelectronic devices.[1−14] They are usually synthesized by the metal catalyzed vapor−liquid−solid (VLS),[2−5,7−10,12,13] solid−vapor,[11] or solvothermal reaction techniques.[6,14]

As a key step towards the realization of their potential in practical applications, it is still necessary to develop new synthetic routes capable of generating uniform 1-D nanostructures in high volumes, together with a controllable size, composition, and single crystallinity. Among other versatile synthetic methods, chemical templating against existing nanostructures offers a very powerful means to increase the compositional diversity of materials or to generate nanostructures that might be difficult or impossible to directly synthesize.[15] The Alivisatos and Xia research groups suc-

* Corresponding author. E-mail: parkjh@korea.ac.kr.

(1) (a) Hu, J.; Odom, T. W.; Lieber, C. M. *Acc. Chem. Res.* **1999**, *32*, 435. (b) Gudiksen, M. S.; Lauhon, L. J.; Wang, J.; Smith, D. C.; Lieber, C. M. *Nature (London, U.K.)* **2002**, *415*, 617.

(2) (a) Barrelet, C. J.; Wu, Y.; Bell, D. C.; Lieber, C. M. *J. Am. Chem. Soc*. **2003**, *125*, 11498. (b) Duan, X.; Huang, Y.; Agarwal, R.; Lieber, C. M. *Nature (London, U.K.)* **2003**, *421*, 241. (c) Barrelet, C. J.; Greytak, A. B.; Lieber, C. M. *Nano Lett.* **2004**, *4*, 1981. (d) Huang, Y.; Duan, X.; Lieber, C. M. *Small* **2005**, *1*, 142. (e) Friedman, R. S.; McAlpine, M. C.; David, S.; Ricketts Ham, D.; Lieber, C. M. *Nature* **2005**, *434*, 1085. (f) Agarwal, R.; Barrelet, C. J.; Lieber, C. M. *Nano Lett.* **2005**, *5*, 917. (g) Barrelet, C. J.; Bao, J.; Lonèar, M.; Park, H. G.; Capasso, F.; Lieber, C. M. *Nano Lett*. **2006**, *6*, 11.

(3) (a) Liu, Y. K.; Zapien, J. A.; Geng, C. Y.; Shan, Y. Y.; Lee, C. S.; Lifshitz, Y.; Lee, S. T. *Appl. Phys. Lett*. **2004**, *85*, 3241. (b) Jie, J. S.; Zhang, W. J.; Jiang, Y.; Meng, X. M.; Li, Y. Q.; Lee, S. T. *Nano Lett*. **2006**, *6*, 1887.

(4) (a) Pan, A.; Liu, D.; Liu, R.; Wang, F.; Zhu, X.; Zou, B. *Small* **2005**, *1*, 980. (b) Pan, A. L.; Liu, R. B.; Zou, B. S. *Appl. Phys. Lett*. **2005**, *88*, 173102.

(5) (a) Gao, T.; Wang, T. *J. Phys. Chem. B* **2004**, *108*, 20045. (b) Gao, T.; Li, Q. H.; Wang, T. H. *Appl. Phys. Lett*. **2005**, *86*, 173105.

(6) (a) Long, Y.; Chen, Z.; Wang, W.; Bai, F.; Jin, A.; Gu, C. *Appl. Phys. Lett*. **2005**, *86*, 153102. (b) Wang, W.; Bai, F. *Appl. Phys. Lett*. **2005**, *87*, 193109.

(7) (a) Titova, L. V.; Hoang, T. B.; Jackson, H. E.; Smith, L. M.; Yarrison-Rice, J. M.; Lensch, J. L.; Lauhon, L. J. *Appl. Phys. Lett*. **2006**, *89*, 53119. (b) Hoang, T. B.; Titova, L. V.; Jackson, H. E.; Smith, L. M.; Yarrison-Rice, J. M.; Lensch, J. L.; Lauhon, L. J. *Appl. Phys. Lett*. **2006**, *89*, 123123.

(8) Ma, R. M.; Dai, L.; Huo, H. B.; Yang, W. Q.; Qin, G. G.; Tan, P. H.; Huang, C. H.; Zheng, J. *Appl. Phys. Lett*. **2006**, *89*, 203120.

(9) (a) Jiang, Y.; Meng, X. M.; Liu, J.; Xie, Z. Y.; Lee, C. S.; Lee, S. T. *Adv. Mater*. **2003**, *15*, 323. (b) Jiang, Y.; Meng, X. M.; Liu, J.; Hong, Z. R.; Lee, C. S.; Lee, S. T. *Adv. Mater.* **2003**, *15*, 1195. (c) Rosenberg, R. A.; Shenoy, G. K.; Heigl, F.; Lee, S. T.; Kim, P. S.; Zhou, X. T.; Sham, T. K. *Appl. Phys. Lett*. **2005**, *86*, 263115. (d) Duo, D.; Ma, D.; Lee, S. T.; Mueller, P.; Alvarado, S. F. *Nano Lett*. **2006**, *6*, 926. (e) Jiang, Y.; Zhang, W. J.; Jie, J. S.; Meng, X. M.; Zapien, J. A.; Lee, S. T. *Adv. Mater*. **2006**, *18*, 1527.

(10) (a) Xiong, Q.; Chen, G.; Acord, J. D.; Liu, X.; Zengel, J.; Gutierrez, H. R.; Redwing, J. M.; Lew Yan Voon, L. C.; Lassen, B.; Eklund, P. C. *Nano Lett.* **2004**, *4*, 1663. (b) Xiong, Q.; Wang, J.; Reese, O.; Lew Yan Voon, L. C.; Eklund, P. C. *Nano Lett.* **2004**, *4*, 1991. (c) Li, X.; Wang, X.; Xiong, Q.; Eklund, P. C. *Appl. Phys. Lett.* **2005**, *87*, 233113. (d) Li, X.; Wang, X.; Xiang, Q.; Eklund, P. C. *Nano Lett.* **2005**, *5*, 1982.

(11) Wang, X.; Gao, P.; Li, J.; Summers, C. J.; Wang, Z. L. *Adv. Mater.* **2002**, 14, 1732. (b) Ma, C.; Moore, D.; Li, J.; Wang, Z. L. *Adv. Mater*. **2003**, *15*, 228. (c) Ding, Y.; Wang, X. D.; Wang, Z. L. *Chem. Phys. Lett*. **2004**, *398*, 32. (d) Wang, Z.; Daemen, L. L.; Zhao, Y.; Zha, C. S.; Downs, R. T.; Wang, X.; Wang, Z. L.; Hemley, R. J. *Nat. Mater*. **2005**, *4*, 922. (e) Moore, D.; Wang, Z. L. *J. Mater. Chem*. **2006**, *16*, 3898. (f) Hao, Y.; Meng, G.; Wang, Z. L.; Ye, C.; Zhang, L. *Nano Lett*. **2006**, *6*, 1650.

(12) (a) Zhu, Y. C.; Bando, Y.; Xue, D. F. *Appl. Phys. Lett*. **2003**, *82*, 1769. (b) Hu, J.; Bando, Y.; Liu, Z.; Zhan, J.; Goldberg, D.; Sekiguchi, T. *Angew. Chem., Int. Ed.* **2004**, *43*, 63. (c) Shen, G.; Bando, Y.; Gao, Y.; Golberg, D. *J. Phys. Chem. B* **2006**, *110*, 14123.

(13) (a) Geng, B. Y.; Zhang, Y. G.; Wang, G.; Xie, T.; Meng, G. W.; Zhang, L. D. *Appl. Phys. A* **2004**, *79*, 1761. (b) Ye, C.; Fang, X.; Li, G.; Zhang, L. *Appl. Phys. Lett*. **2004**, *85*, 3035. (c) Fang, X. S.; Ye, C. H.; Zhang, L. D.; Wang, Y. H.; Wu, Y. C. *Adv. Funct. Mater*. **2005**, *15*, 63. (d) Ye, C.; Fang, X.; Wang, M.; Zhang, L. *J. Appl. Phys*. **2006**, *99*, 63504.

(14) Lu, F.; Cai, W.; Zhang, Y.; Li, Y.; Sun, F. *Appl. Phys. Lett*. **2006**, *89*, 231928.

10.1021/cm070814f CCC: $37.00
Published on Web 08/22/2007

cessfully applied this method to cation exchange reactions in solution.[16,17] Könenkamp and co-workers reported the use of an anion exchange reaction to convert ZnO nanotubular columns into ZnS in the gas phase.[18] They also demonstrated the further transformation of ZnS into Cu_2S, Ag_2S, Bi_2S_3, etc. in solution. Recently, the transformation of mesoporous CdS into CuS via cation exchange in solution was reported by Han and co-workers.[19] However, to the best of our knowledge, no cation exchange reaction in the gas phase has been developed to synthesize 1-D nanostructures.

Herein, we report on the chemical conversion (i.e., cation exchange) reactions between CdS nanobelts and ZnS nanobelts in the gas phase. The single-crystalline wurtzite CdS nanobelts (NBs) transform completely into single-crystalline wurtzite ZnS NBs. On the contrary, the ZnS NBs transform incompletely into CdS NBs under our experimental conditions. As a result, single-crystalline wurtzite Cd-doped ZnS nanobelts (i.e., $Zn_{0.95}Cd_{0.05}S$ and $Zn_{0.4}Cd_{0.6}S$) were produced instead. 3-D CdS−ZnO nanobelt−nanowire hetero-nanostructures grew at temperatures lower than the conversion temperature. These results provide insight into the mechanism of the substitution reaction of 1-D nanostructures in the gas phase.

Experimental Procedures

For the synthesis of the CdS NBs, CdS (99.98%, Aldrich) powders were placed a few centimeters apart from an Au nanoparticle-deposited Si substrate inside a quartz tube reactor. As the source was evaporated at 850 °C for 1 h under argon flow, high-density CdS NBs were deposited on the substrates at about 700 °C. For the conversion of the CdS NBs into the ZnS NBs, the pre-grown CdS NBs were placed in the reactor, and Zn powders were evaporated at temperatures in the range of 500−1000 °C. The ZnS NBs were synthesized on an Au nanoparticle-deposited Si substrate by the evaporation of ZnO (99.98%, Aldrich)/NiS (99%, Aldrich) powders at 1100 °C. The substrates were placed a few centmeters apart from the Cd source inside the reactor at a temperature of 900 °C. For the conversion of the ZnS NBs into CdS NBs, the pre-grown ZnS NBs were placed inside the reactor, and the Cd powders were evaporated at temperatures in the range of 500−1000 °C.

The products were analyzed by scanning electron microscopy (SEM, Hitachi S-4700), field-emission transmission electron microscopy (TEM, FEI TECNAI G^2 200 kV and Jeol JEM 2100F), high-voltage TEM (HVTEM, Jeol JEM ARM 1300S, 1.25 MV), electron diffraction (ED), and energy-dispersive X-ray fluorescence spectroscopy (EDX). High-resolution X-ray diffraction (XRD) patterns were obtained using the 8C2 beam line of the Pohang Light Source (PLS) with monochromatic radiation (λ = 1.54520 Å). Temperature-dependent steady-state photoluminescence (PL) measurements were carried out using a He−Cd laser (λ = 325 nm) and a Nd:YAG laser (λ = 266 nm) as the excitation sources.

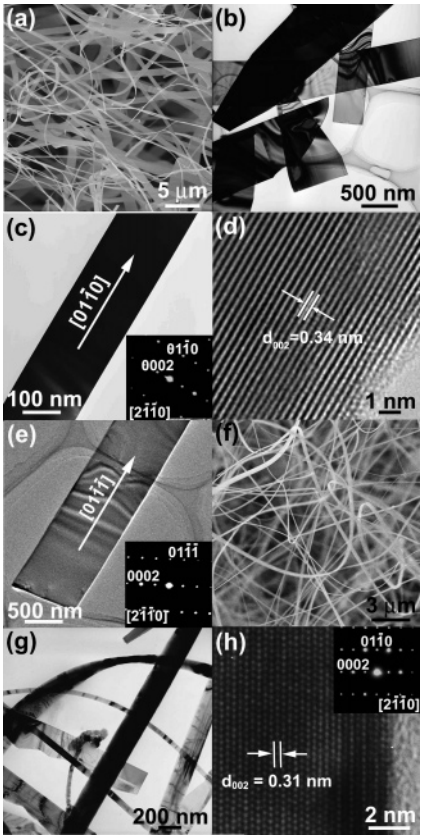

Figure 1. (a) SEM micrograph showing the high-density CdS NBs on the substrate. (b) TEM image showing the general morphology of the CdS NBs (av width = 400 nm). (c) HRTEM image of the CdS NB grown in the [01$\bar{1}$0] growth direction. The SAED pattern confirms the single crystallinity and growth direction (inset). (d) Distance between neighboring (002) planes is 3.4 Å. (e) TEM image showing another CdS NB grown in the [01$\bar{1}\bar{1}$] growth direction. (f) SEM micrograph of the high-density ZnS NBs. (g) TEM image showing the general morphology of the ZnS NBs. Their average width is 200 nm. (h) Lattice-resolved image of the nanobelts grown in the [01$\bar{1}$0] growth direction. The distance between the neighboring (002) planes is 3.1 Å. Its corresponding SAED pattern reveals the [01$\bar{1}$0] growth direction (inset).

Results and Discussion

Figure 1a shows the SEM image of the high-density belt-like CdS nanostructures synthesized by the thermal evaporation of CdS powders. Their length reaches about 50 μm. The TEM image reveals that they have a smooth flat surface without any nanoparticle impurities (Figure 1b). Their width is in the range of 200−500 nm (av = 400 nm). The HRTEM image shows a highly crystalline nanobelt grown in the [01$\bar{1}$0] direction (Figure 1c). The corresponding selected-area ED (SAED) pattern, measured at the [2$\bar{1}\bar{1}$0] zone axis, confirms the [01$\bar{1}$0] growth direction. Figure 1d shows the corresponding lattice-resolved image revealing the perfect crystalline nature of the nanobelt. The (002) fringes are separated by a distance of about 3.4 Å, which is close to that of the wurtzite CdS crystal (a = 4.14092 Å and c = 6.7198 Å; JCPDS Card No. 41−1049). Figure 1e displays the TEM image and SAED pattern (inset) of another CdS NB having the [01$\bar{1}\bar{1}$] growth direction. Its end edge is not

(15) Xia, Y.; Yang, P. *Adv. Mater.* **2005**, *15*, 353.
(16) Son, D. H.; Hughes, S. M.; Yin, Y.; Alivisatos, P. A. *Science* **2004**, *306*, 1009.
(17) (a) Gates, B.; Wu, Y.; Yin, Y.; Yang, P.; Xia, Y. *J. Am. Chem. Soc.* **2001**, *123*, 11500. (b) Sun, Y.; Mayers, B.; Xia, Y. *Adv. Mater.* **2001**, *123*, 11500. (c) Sun, Y.; Xia, Y. *J. Am. Chem. Soc.* **2004**, *126*, 3892. (d) Jeong, U.; Camargo, P. H.; Lee, Y. H.; Xia, Y. *J. Mater. Chem.* **2006**, *16*, 3893.
(18) (a) Dloczik, L.; Engelhardt, R.; Ernst, K.; Fiechter, S.; Sieber, I.; Könenkamp, R. *Appl. Phys. Lett.* **2001**, *78*, 3687. (b) Dloczik, L.; Engelhardt, R.; Ernst, K.; Lux-Steiner, M. C.; Könenkamp, R. *Sens. Actuators, B* **2002**, *84*, 33. (c) Dloczik, L.; Könenkamp, R. *Nano Lett.* **2003**, *3*, 651. (d) Dloczik, L.; Lux-Steiner, M. C.; Könenkamp, R. *Thin Solid Films* **2003**, *431*, 131.
(19) Lubeck, C. R.; Han, Y.-J.; Gash, A. E.; Satcher, J. H., Jr. *Adv. Mater.* **2006**, *18*, 781.

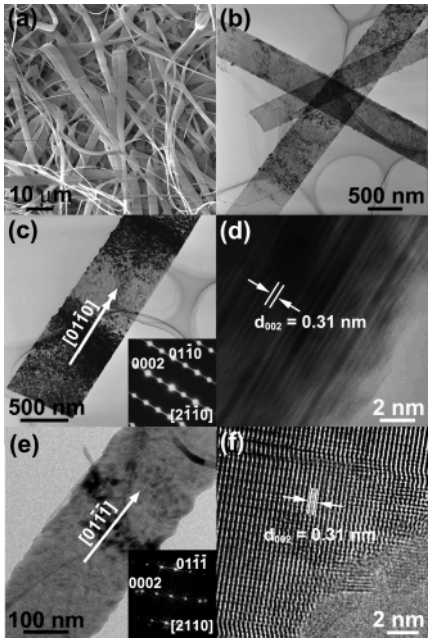

Figure 2. (a) SEM micrograph showing the high-density ZnS NBs synthesized by the conversion reaction of the CdS NBs. (b) TEM image showing the general morphology of the ZnS NBs. The average width is 400 nm. (c) TEM image of the ZnS NBs having a [01$\bar{1}$0] growth direction. (d) Lattice-resolved image reveals the stacking faults along the [0001] direction. The (002) fringes are separated by a distance of about 3.1 Å, which is close to that of wurtzite ZnS crystal. The corresponding SAED pattern confirms the [01$\bar{1}$0] growth direction. (e) TEM image of the ZnS NBs having a [01$\bar{1}\bar{1}$] growth direction. (f) Lattice-resolved image reveals the (002) fringes separated by a distance of about 3.1 Å and their stacking faults. The corresponding FFT ED pattern confirms the [01$\bar{1}\bar{1}$] growth direction.

perpendicular to the growth direction, but has a tilt angle of ~10°. The CdS NBs are usually skewed at the end part, as shown in the TEM image of Figure 1b. We observed that most of the CdS NBs have either a [01$\bar{1}$0] or a [01$\bar{1}\bar{1}$] growth direction.

Figure 1f shows the SEM image of the ZnS NBs synthesized directly by the thermal evaporation of ZnO/NiS powders. Their length is about 50 μm. The TEM image reveals that their width is in the range of 100−300 nm (av = 200 nm) (Figure 1g). The average width is about 2 times smaller than that of the CdS NBs (400 nm). Their side edges are occasionally one-sided and saw-toothed. The HRTEM image shows a highly crystalline nanobelt grown in the [01$\bar{1}$0] direction (Figure 1h). The (002) fringes are separated by a distance of about 3.1 Å, which is close to that of the wurtzite ZnS crystal (a = 3.82098 Å and c = 6.2573 Å; JCPDS Card No. 36−1450). Its corresponding SAED pattern at the [2$\bar{1}\bar{1}$0] zone axis confirms the [01$\bar{1}$0] growth direction (Figure 1h, inset). All of the ZnS NBs that we observed have a [01$\bar{1}$0] growth direction. The XRD and PL data confirm the formation of high-purity CdS and ZnS NBs, as is described next.

Figure 2a shows the SEM image of the ZnS NBs synthesized by the conversion reaction of the CdS NBs (shown in Figure 1a−e). The conversion of the CdS NBs to the ZnS NBs takes place completely during the 30 min period of evaporation of the Zn powders at 800 °C. The TEM image reveals that a huge number of humps cover the top surface and that the side edges are not smooth, which distinguishes them from the CdS NB templates (Figure 2b). Their average width is still 400 nm even after the conversion. The TEM image shows a highly crystalline ZnS NB grown in the [01$\bar{1}$0] direction (Figure 2c). The lattice-resolved image of the side edge part reveals the presence of stacking faults along the [0001] direction (Figure 2d). The corresponding SAED pattern, taken at the [2$\bar{1}\bar{1}$0] zone axis, shows the defective crystalline nature of the [0001] planes. The (002) fringes are separated by a distance of about 3.1 Å, which is close to that of wurtzite ZnS crystal. Figure 2e shows another ZnS NB having a [01$\bar{1}\bar{1}$] growth direction. Its corresponding fast-Fourier transform ED (FFT ED) pattern, generated from the inversion of the TEM image using DigitalMicrograph GMS1.2 software (Gatan Inc.), confirms the [01$\bar{1}\bar{1}$] growth direction and the defects along the [0001] direction. Figure 2f corresponds to the lattice-resolved image for its side edge. The (002) fringes are separated by a distance of about 3.1 Å, which is close to that of wurtzite ZnS crystal. We observed that the width and growth direction of the wurtzite ZnS NBs remain the same as those of the wurtzite CdS NBs but that there are stacking faults along the [0001] direction and a bumpy surface, probably due to the substitution reaction. The EDX data show no trace of the Cd element in the ZnS NBs (Supporting Information Figure S1). We refer to this sample as A.

Next, the ZnS NBs (as shown in Figure 1f−h) were reacted with Cd vapor at 1000 °C. The ZnS NBs cannot completely transform into CdS NBs in the presence of Zn powders evaporated for 1 h. Instead, Cd-doped ZnS nanobelts (i.e., $Zn_{0.95}Cd_{0.05}S$ and $Zn_{0.4}Cd_{0.6}S$) were synthesized as the products after reaction times of 10 min and 1 h, respectively. Using a longer reaction time or a higher reaction temperature (1200 °C) is detrimental to the morphology of the ZnS NBs. Figure 3a shows the SEM image of the high-density $Zn_{0.95}Cd_{0.05}S$ NBs. The TEM image reveals that their diameter remains in the range of 100−300 nm, which is same as that of the ZnS NBs, after the Cd substitution (Figure 3b). Figure 3c corresponds to the lattice-resolved image of an individual nanobelt, showing that the highly crystalline (002) fringes are separated by a distance of about 3.1 Å, which is close to that of wurtzite ZnS crystal. The SAED pattern confirms the [01$\bar{1}$0] growth direction, maintained after the Cd substitution (Figure 3c, inset). The EDX line scanning analysis indicates that the average Cd content (x = [Cd]/([Zn] + [Cd])) of the individual nanowires is about x = 0.05 (±10% uncertainty), with a uniform distribution of the elements along the cross-section (Figure 3d). The EDX data are shown in the Supporting Information Figure S1. We refer to this sample as B.

Figure 3e shows the SEM image of the high-density $Zn_{0.4}Cd_{0.6}S$ NBs. Figure 3f corresponds to a TEM image showing the general morphology of the $Zn_{0.4}Cd_{0.6}S$ NBs. Their average width is 200 nm. Figure 3g shows a lattice-resolved image revealing the single-crystalline nature of the nanobelts. The FFT ED pattern confirms the [01$\bar{1}$0] direction (Figure 3g, inset). The (002) fringes are separated by a distance of about 3.1 Å. The EDX line scanning reveals that the 60% Cd is distributed homogeneously over the whole cross-section of the nanobelt (Figure 3h). The width and growth direction

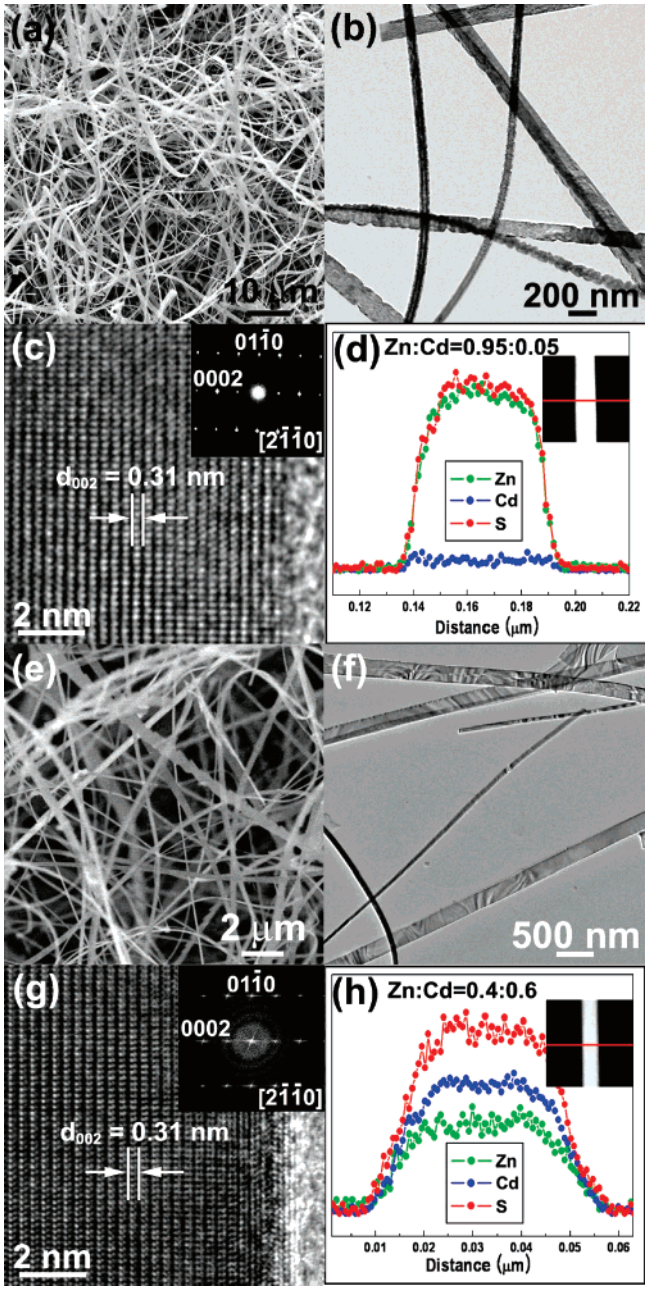

Figure 3. (a) SEM micrograph showing high-density $Zn_{0.95}Cd_{0.05}S$ NBs. (b) TEM image revealing the general morphology of the nanobelts. Their average diameter is 200 nm. (c) Lattice-resolved image of an individual nanobelt, revealing the highly crystalline (002) fringes separated by a distance of about 3.1 Å parallel to the growth direction [01$\bar{1}$0]. The SAED pattern confirms that the single-crystalline wurtzite ZnS crystal grew in the [01$\bar{1}$0] direction (inset). (d) EDX line scanning reveals the uniform distribution of Zn, S, and Cd ([Cd]/([Zn] + [Cd]) = 0.05) along the cross-section. (e) SEM micrograph showing the high-density $Zn_{0.4}Cd_{0.6}S$ NBs. (f) TEM image revealing their nanobelt morphology. (g) Lattice-resolved image revealing their single-crystalline nature. The (002) fringes are separated by a distance of about 3.1 Å. The FFT ED pattern confirms the single-crystalline wurtzite structured ZnS nanocrystal grown in the [01$\bar{1}$0] direction (inset). (h) EDX line scanning reveals that the 60% Cd element is homogeneously distributed over the cross-section of the nanobelts.

remain the same as those of the ZnS NBs. The corresponding EDX data, as well as the XRD and PL data, confirm the production of the Cd-doped ZnS NBs, as shown in the Supporting Information Figure S1 and in Figures 5 and 6. We refer to this sample as C.

To our best knowledge, this is probably the first attempt of a cation substitution reaction from CdS to ZnS nanostructures (and vice versa). The result indicates that the complete conversion of the CdS NBs to the ZnS NBs occurs using Zn vapor transport at 800 °C, while the reverse reaction is incomplete using Cd vapor transport even at 1000 °C. Although the vapor pressure of Zn (~0.5 atm) at 800 °C is even lower than that of Cd (~1 atm), the substitution reaction of Cd with Zn takes place more efficiently, as compared to the opposite reaction in which Cd substitutes Zn. Therefore, we conjectured that the mobility of the cations can be an important factor in determining the rate of the substitution reaction in the gas phase. The smaller radius and lighter mass of Zn ($r(Zn^{2+}) = 74$ pm and $m_{Zn} = 65.4$ amu) would have a higher mobility than the larger radius and heavier mass of Cd ($r(Cd^{2+}) = 92$ pm and $m_{Cd} = 112.4$ amu). Then the higher mobility Zn could substitute Cd well at lower temperatures, as compared to the opposite case. Moreover, the enthalpy of formation was reported to be −206 and −149 kJ/mol, respectively, for ZnS and CdS.[20] The conversion reaction CdS → ZnS is thus more thermodynamically preferred than the opposite reaction. Therefore, the conversion reaction CdS → ZnS NBs would be more favorable kinetically and thermodynamically, as compared to the ZnS → CdS NBs reaction.

The synthesis of $Zn_{1-x}Cd_xS$ nanocrystals or nanowires by one-step solvothermal or chemical vapor deposition methods has been reported by a number of research groups.[21−25] These one-step syntheses showed that the Cd doping of ZnS usually shifts the band gap to a lower energy and increases the lattice constants. However, the present nanobelts synthesized by the substitution reaction of Zn with Cd exhibit no significant change in their lattice constants or their band gap, even in the case of ~60% Cd incorporation, as described next. The incomplete substitution of Zn with Cd is most probably related to the lack of change of the lattice constants.

At temperatures (500 °C) lower than the complete conversion temperature (800 °C) of CdS NBs → ZnS NBs, we observed the formation of novel 3-D branched heteronanostructures, in which the ZnO nanowalls (NWs) grew as branches on the CdS NB backbones. Figure 4ashows the SEM micrograph of a high-density ZnO−CdS nanostructure synthesized by the thermal evaporation of Zn powders, showing that the ZnO NWs completely covered the surface of the CdS NBs. The magnified SEM image shows that the ZnO NWs align well on the surface of the nanobelts, especially on the side edge (Figure 4b). The length of the ZnO NWs is 1−2 μm. The HVTEM image reveals that the ZnO NWs grew directly on the side edge of the CdS NBs (Figure 4c). The average diameter of the aligned ZnO NWs is 50 nm. The two insets in Figure 4c show the FFT ED patterns for the CdS NBs and ZnO NWs, respectively. The [0001] direction of the ZnO NWs coincides exactly with the

(20) Demore, S.; Navrotsky, A. *Am. Mineral.* **2006**, *91*, 400.
(21) Liu, Y.; Zapien, J. A.; Shan, Y. Y.; Geng, C. -Y.; Lee, C. S.; Lee, S.-T. *Adv. Mater.* **2005**, *17*, 1372.
(22) Li, Y.; Ye, M.; Yang, C.; Li, X.; Li, Y. *Adv. Funct. Mater.* **2005**, *15*, 433.
(23) Hsu, Y.-J.; Lu, S.-Y.; Lin, Y.-F. *Adv. Funct. Mater.* **2005**, *15*, 1350.
(24) Zhai, T.; Gu, Z.; Yang, W.; Zhang, X.; Huang, J.; Zhao, Y.; Yu, D.; Fu, H.; Ma, Y.; Yao, J. *Nanotechnology* **2006**, *17*, 4644.
(25) Liu, J. Z.; Yan, P. X.; Yue, G. H.; Chang, J. B.; Qu, D. M.; Zhuo, R. F. *J. Phys. D: Appl. Phys.* **2006**, *39*, 2352.

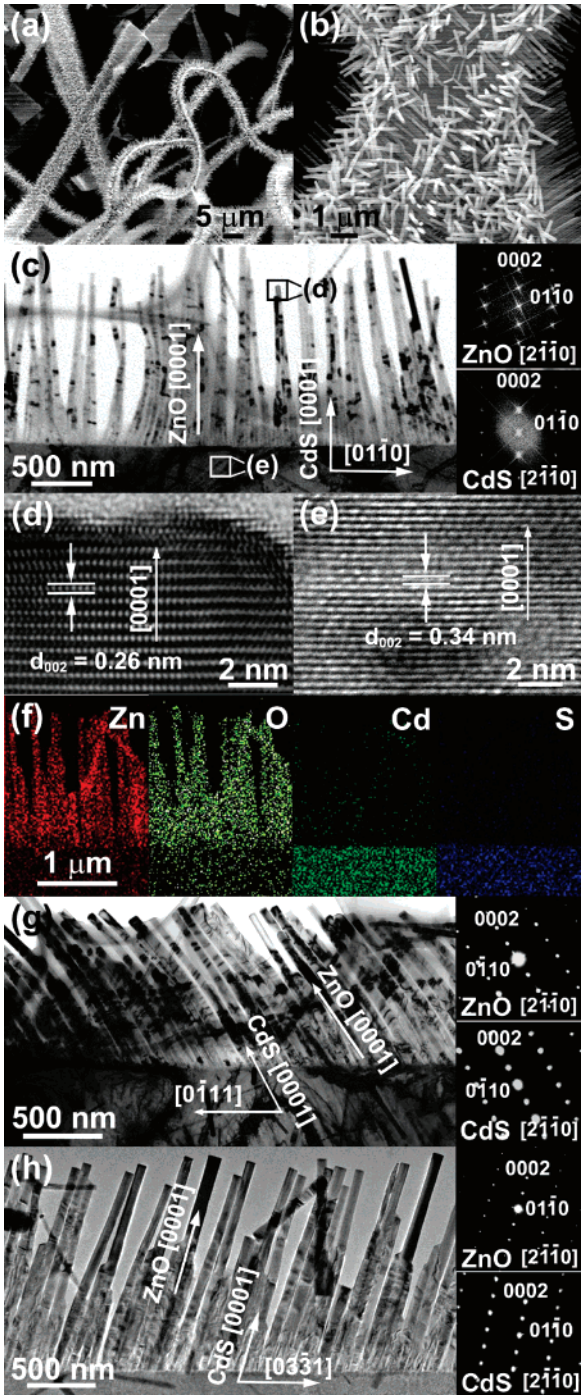

Figure 4. (a) SEM micrograph showing the ZnO−CdS hetero-nanostructure in which the high-density ZnO NWs covered the CdS NBs. (b) Magnified SEM image showing the aligned ZnO NWs on the surface of the nanobelts, especially on the side edge. (c) HRTEM image reveals that the well-aligned ZnO NWs (av diameter = 50 nm and length = 1.5 μm) grew directly on the side edge of the CdS NBs. The two insets correspond to the FFT ED patterns for the CdS and ZnO, showing their matched [0001] direction. The ZnO NWs align to the vertical direction of the CdS NBs. (d) HRTEM image of the high-crystalline ZnO NWs grown in the [0001] direction. The (002) fringes are separated by a distance of about 2.6 Å. (e) HRTEM image of the CdS NBs showing the [0001] direction parallel to the [0001] direction of the ZnO NWs. The (002) fringes are separated by a distance of about 3.4 Å. (f) EDX elemental mapping of Zn, O, Cd, and S. (g) Another CdS−ZnO nanostructure in which the ZnO NWs are tilted at an angle of ~30° with respect to the vertical direction of the CdS NBs. The corresponding SAED pattern confirms the coincident [0001] directions of ZnO and CdS (insets). (h) [0001] directions of the ZnO NWs are tilted at an angle of 15° with respect to the vertical direction of the CdS NBs. The corresponding SAED pattern confirms the coincident [0001] directions of ZnO and CdS (insets).

[0001] direction of the CdS NBs, whose growth direction is [01$\bar{1}$0]. The ZnO NWs are vertically aligned with respect to the [01$\bar{1}$0] growth direction of the CdS NBs. The CdS NBs are still single-crystalline without any defects.

The lattice-resolved TEM image (for the marked area in Figure 4c) shows the high-crystalline ZnO NWs grown in the [0001] direction (Figure 4d). The (002) fringes are separated by a distance of about 2.6 Å, which is close to that of wurtzite ZnO crystal (a = 3.24982 Å and c = 5.20661 Å; JCPDS Card No. 36−1451). Another lattice-resolved TEM image (for the marked area in Figure 4c) shows the high-crystalline CdS NBs (Figure 4e). The (002) fringes are separated by a distance of about 3.4 Å, which is close to that of wurtzite CdS crystal. Figure 4f displays the EDX elemental mapping of Zn, O, Cd, and S of another CdS−ZnO nanostructure, respectively. These nanowire teeth (hereafter referred to as nanoteeth) consisted of Zn and O, but the nanobelts were composed of only Cd and S elements. The corresponding EDX data are shown in the Supporting Information Figure S1.

Figure 4g shows the TEM image of another CdS−ZnO hybrid nanostructure. The insets in Figure 4g correspond to the SAED patterns for the CdS NBs and ZnO NWs, respectively, showing that the [0001] direction of the ZnO NWs virtually coincides with the [0001] direction of the CdS NBs, whose growth direction is [0$\bar{1}$11]. These ZnO NWs are not vertically aligned with the growth direction of the CdS NBs but are tilted from the vertical direction at an angle of about 30°. Figure 4h shows the TEM image of another CdS−ZnO hybrid nanostructure. The insets in Figure 4h display the SAED patterns for the CdS NBs and ZnO NWs, respectively, revealing that the [0001] direction of the ZnO NWs nearly matches the [0001] direction of the CdS NBs. The side edge is parallel to the [03$\bar{3}$1] direction, corresponding to the skewed edge of the CdS NBs having a [01$\bar{1}$0] growth direction. The ZnO NWs are not vertically aligned with this [03$\bar{3}$1] direction but are slanted at an angle of ~15°. We refer to this sample as D. The XRD and PL data confirm the synthesis of ZnO NWs on the CdS NBs (as shown in Figures 5 and 6).

The synthesis of the ZnO NW assembled hierarchical heterostructures was demonstrated for CNTs and various nanowires.[26−28] ZnO NWs are usually vertically aligned on the lateral surface of the nanowires. In the case of the epitaxial growth of CdS NWs on Au-deposited ZnS NWs, the CdS NW branches were vertically aligned on the ZnS NW backbones.[29] In contrast, the present CdS−ZnO heterostructures show a remarkable feature in that the ZnO NWs can be aligned in a direction that is tilted with respect to the vertical direction of the CdS NBs and that the [0001] direction of the ZnO NWs always matches that of the CdS NBs. We observed that the CdS NBs have either one-sided or double-sided ZnO nanoteeth. For the growth of ZnO, ZnS, and CdSe nanosaws/nanoteeth, Wang and co-workers sug-

(26) Lao, J. Y.; Wen, J. G.; Ren, Z. F. *Nano Lett.* **2002**, *2*, 1287.
(27) Bae, S. Y.; Seo, H. W.; Choi, H. C.; Park, J.; Park, J. *J. Phys. Chem. B* **2004**, *108*, 12318.
(28) Shen, G.; Chen, D.; Lee, C. J. *J. Phys. Chem. B* **2006**, *110*, 15689.
(29) Jung, Y.; Ko, D.-K.; Agarwal, R. *Nano Lett.* **2007**, *7*, 264.

gested that the catalytically more active cation (Zn^{2+} or Cd^{2+})-terminated (0001) surface is responsible for the growth of the toothed morphology.[30,31] We therefore suggest that the Cd-terminated (0001) active polar surface supplies the sites for the deposition of the polar ($000\bar{1}$) surface of ZnO, producing ZnO NWs aligned along their [0001] direction.

The growth of the ZnO NWs would be expected to be initiated by the deposition of nanosized Zn droplets on the surface of the CdS NBs. If the diffusion rate of Zn in the CdS nanocrystals is negligibly small at 500 °C, the residual O could dissolve into the Zn droplets and precipitate so as to grow the ZnO NWs according to the vapor-liquid-solid (VLS) mechanism. The completely converted ZnS NBs (from CdS NBs) have uneven surfaces (as shown in Figure 2), providing evidence that the deposition of Zn initiates the exchange reaction. If the diffusion rate of Zn in the CdS nanocrystals is fast enough to replace the Cd sites (at the higher temperature), then CdS would transform into ZnS NBs. We noticed the presence of a considerable amount of defects along the [0001] direction (as shown in Figure 3) in the case of the transformed ZnS NBs (from the CdS NBs). The preferred [0001] growth of the ZnO NWs (in the CdS−ZnO heterostructures), as well as the presence of defects along the [0001] direction, offer insight into the reaction mechanism in which the cation replacement reaction may occur preferentially through the polar (0001) surface of wurtzite CdS (or ZnS).

Figure 5 displays the XRD pattern of CdS NBs, ZnS NBs, ZnO NWs (synthesized as described in ref 26), and ZnS NBs (A), $Zn_{0.95}Cd_{0.05}S$ NBs (B), $Zn_{0.4}Cd_{0.6}S$ NBs (C), and CdS−ZnO nanostructures (D). The XRD pattern of the CdS and ZnS NBs (and spectrum A) confirms that their structure corresponds to that of the high-crystalline wurtzite CdS and ZnS crystals, respectively, without the formation of other oxide phases. The Cd-doped ZnS NBs (spectra B and C) show only wurtzite ZnS peaks, confirming the maintenance of the ZnS structure. The peak position shifts negligibly relative to that of the ZnS NBs, although the Cd concentration increases to 60%. This result is inconsistent with the prediction that the substitution of the Zn^{2+} ions ($r(Zn^{2+}) = 0.74$ Å) with the larger radius Cd^{2+} ions ($r(Cd^{2+}) = 0.92$ Å) expands the lattice constants of ZnS. As mentioned previously, this unchanged lattice constant would be responsible for the incomplete substitution of Zn with Cd. The absence of any increase of the peak width implies that the Cd incorporation does not deteriorate significantly the crystallinity of the ZnS NBs. The CdS−ZnO hybrid nanostructures (spectrum D) show all CdS peaks as well as ZnO (101) and (102) peaks.

Figure 6 shows room-temperature steady-state PL spectra of CdS NBs, ZnS NBs, ZnO NWs, ZnS NBs (A), $Zn_{0.95}Cd_{0.05}S$ NBs (B), $Zn_{0.4}Cd_{0.6}S$ NBs (C), and CdS−ZnO nanostructures (D). For ZnS NBs (spectra A−C), the excitation wavelength is 266 nm (4.66 eV). For CdS NBs, ZnO NWs, and spectrum D, the excitation wavelength is 325 nm (3.815 eV). The CdS NBs exhibit a band-edge emission

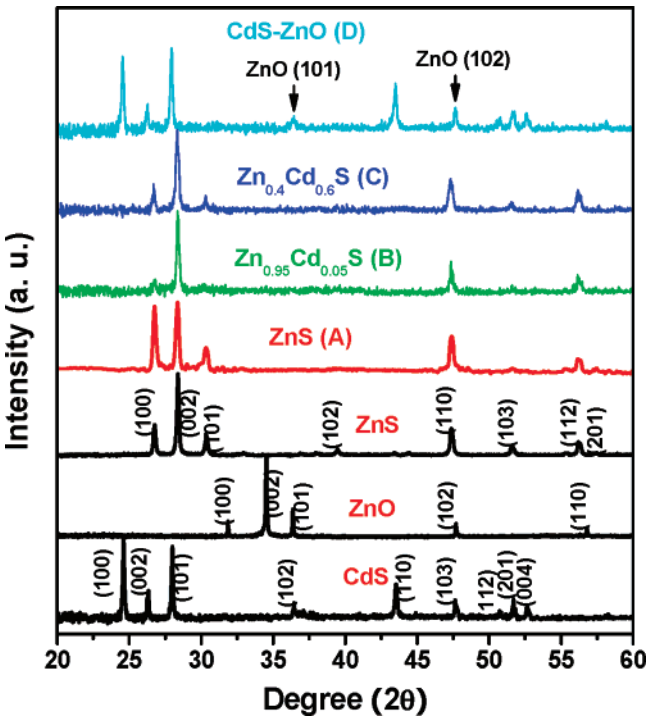

Figure 5. XRD pattern of the CdS NBs, ZnS NBs, ZnO NWs, and ZnS NBs (A), $Zn_{0.95}Cd_{0.05}S$ NBs (B), $Zn_{0.4}Cd_{0.6}S$ NBs (C), and CdS−ZnO nanostructures (D).

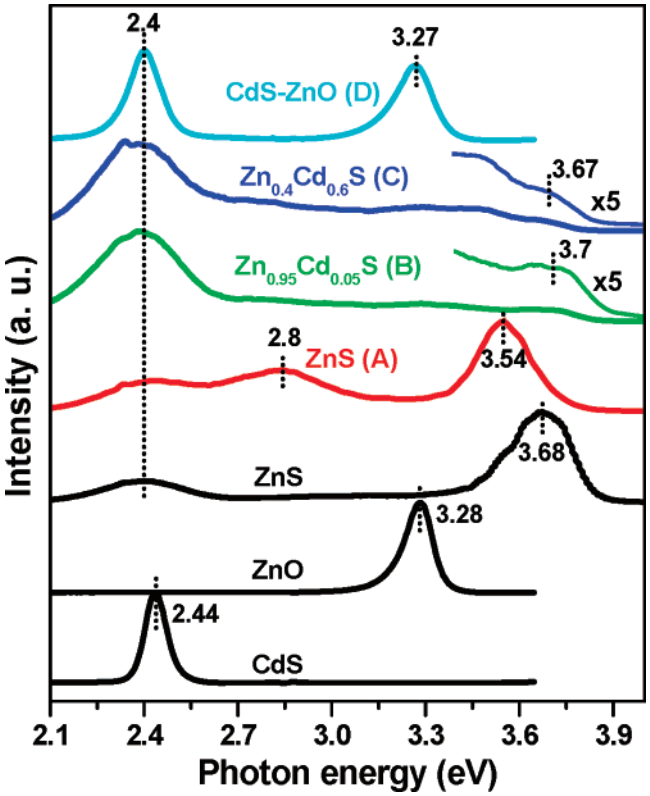

Figure 6. Room-temperature PL spectrum of the CdS NBs, ZnS NBs, ZnO NWs, and ZnS NBs (A), $Zn_{0.95}Cd_{0.05}S$ NBs (B), $Zn_{0.4}Cd_{0.6}S$ NBs (C), and CdS−ZnO nanostructures (D). For the ZnS NBs (A−C), the excitation wavelength is 266 nm (4.66 eV). For the CdS NBs, ZnO NWs, and spectrum D, the excitation wavelength is 325 nm (3.815 eV).

(30) (a) Yan, H.; He, R.; Johnson, J.; Law, M.; Saykally, R. J.; Yang, P. *J. Am. Chem. Soc.* **2003**, *125*, 4728. (b) Wang, Z. L.; Kong, X. Y.; Zuo, J. M. *Phys. Rev. Lett.* **2003**, *91*, 185502. (c) Lao, C. S.; Gao, P. X.; Yang, R. S.; Zhang, Y.; Dai, Y.; Wang, Z. L. *Chem. Phys. Lett.* **2006**, *417*, 358.

(31) (a) Ma, C.; Moore, D.; Li, J.; Wang, Z. L. *Adv. Mater.* **2003**, *15*, 228. (b) Ding, Y.; Ma, C.; Wang, Z. L. *Adv. Mater.* **2004**, *16*, 1740. (c) Ma, C.; Ding, Y.; Moore, D.; Wang, X.; Wang, Z. L. *J. Am. Chem. Soc.* **2004**, *126*, 708.

peak at 2.44 eV.[32] For the ZnO NWs, the emission peak at 3.28 eV is assigned to their band-edge emission.[33] We assigned the 3.68 eV peak of the ZnS NBs to the band-edge emission.[10a] Spectrum A shows a band-edge emission at a lower energy than that of the ZnS NBs, 3.54 eV, which could be related to the reduced band gap caused by the Cd residual (although EDX data reveal no Cd elements) in these NBs. The broad emissions at 2.8 and 2.4 eV might originate from the Cd-doping related defects in the ZnS lattices. Spectra B and C show a drastically reduced band-edge emission of ZnS (position is ~3.7 eV) but a broad emission at 2.4 eV. The band-edge emission is magnified to show the unchanged peak position. The enhanced green emission might originate from the Cd dopant-induced defects in the ZnS lattices. Nevertheless, the appearance of this emission needs further investigation. Spectrum D shows strong peaks at 3.26 and 2.4 eV, which originate from the ZnO NWs and CdS NBs, respectively. These hybrid structures could be used as a distinctive multicolored (blue and green) light-emitting diode nanomaterial.

Conclusion

We synthesized single-crystalline CdS and ZnS NBs and then attempted to interconvert them by a vapor transport method. The average width of the CdS NBs (400 nm) is about 2 times larger than that of the ZnS NBs (200 nm). The $[01\bar{1}0]$ or $[0\bar{1}11]$ growth direction was observed for the CdS NBs, but only $[01\bar{1}1]$ was observed for the ZnS NBs. The Cd and Zn vapors were supplied by the thermal evaporation of Cd and Zn powders, respectively. The single-crystalline wurtzite CdS NBs undergo conversion into wurtzite ZnS NBs at 800 °C. However, the ZnS NBs cannot completely transform into CdS NBs under our experimental conditions (up to 1000 °C). We successfully synthesized $Zn_{0.95}Cd_{0.05}S$ and $Zn_{0.4}Cd_{0.6}S$ NBs by controlling the reaction time. The belt width and growth direction remain unchanged after the conversion reaction. These results indicate that the conversion reaction CdS → ZnS NBs occurs more efficiently, as compared to the opposite substitution (ZnS → CdS NBs). We suggested that the conversion reaction CdS → ZnS NBs in the gas phase could be more favorable from both thermodynamic and kinetic points of view. The 3-D CdS−ZnO nanobelt−nanowire heterostructures grew at a temperature (500 °C) lower than the complete conversion temperature. The ZnO NWs are aligned so that their [0001] direction is matched with that of the CdS NBs, probably due to the polarity of the (0001) surface of the wurtzite structure. The cation replacement reaction may occur through the polar (0001) surface of wurtzite CdS (or ZnS).

Acknowledgment. This work was supported by KRF (R14-2003-033-01003-0 and R02-2004-000-10025-0) and BK21. The SEM, field-emission TEM, HVTEM, and SQUID measurements were performed at the Korea Basic Science Institute. The experiments at PLS were supported in part by MOST and POSTECH.

Supporting Information Available: EDX data of ZnS NBs (synthesized from the conversion of CdS NBs) and $Zn_{0.95}Cd_{0.05}S$ and $Zn_{0.4}Cd_{0.6}S$ NBs. This material is available free of charge via the Internet at http://pubs.acs.org.

CM070814F

(32) (a) Thomas, D. G.; Hopfield, J. J. *Phys. Rev.* **1962**, *128*, 2135. (b) Na, C. W.; Han, D. S.; Kim, D. S.; Kang, Y. J.; Lee, J. Y.; Park, J.; Oh, D. K.; Kim, K. S.; Kim, D. *J. Phys. Chem. B* **2006**, *110*, 6699.

(33) (a) Kong, Y. C.; Yu, D. P.; Zhang, B.; Fang, W.; Feng, S. Q. *Appl. Phys. Lett.* **2001**, *78*, 407. (b) Park, W. I.; Jun, Y. H.; Jung, S. W.; Yi, G. C. *Appl. Phys. Lett.* **2003**, *82*, 964. (c) Bae, S. Y.; Choi, H. C.; Na, C. W.; Park, J. *Appl. Phys. Lett.* **2005**, *86*, 33102.